Frequency Selective Surfaces in the GHz and THz Region: Analysis and Experimental Results

Maurizio Bozzi and Luca Perregrini

Department of Electronics, University of Pavia
Via Ferrata 1, 27100 Pavia, Italy

ABSTRACT

This paper presents a review of our activity in the field of frequency selective surfaces operating both in the GHz and in the THz region, and gives an overview of the state-of-the-art in this research field. A brief description is given of the applications of the frequency selective surfaces in different frequency bands and of the most used configurations. The possible fabrication technologies and the measurement techniques are discussed, along with the numerical methods for the analysis of frequency selective surfaces: a particular emphasis is given to the hybrid Method of the Moment/Boundary Integral-Resonant Mode Expansion method, recently developed at the University of Pavia. Some experimental results are also reported.

Keywords: Frequency selective surfaces, quasi-optical filters, numerical analysis of periodic structures, Boundary Integral-Resonant Mode Expansion method.

1. INTRODUCTION

Frequency Selective Surfaces (FSSs) find many applications from the microwave to the THz region, for both scientific and commercial purposes: they span from antenna systems for radio-astronomy research to the screen doors of the microwave ovens, as discussed in Sec. 2.1.

FSSs in the GHz and THz region tipically consist of metal screens perforated periodically with apertures.[1-3] The shape of the apertures, their size and spacing, and the thickness of the metal screens determine the frequency behavior of the structure. The most common apertures have rectangular or circular shape; cross-shaped apertures are also used. More complicated shapes and multi-screen configurations are sometimes used, in order to achieve a specific performance or to satisfy very tight design specs. Some of these configurations are described in Sec. 2.2.

Many methods for the theoretical analysis of FSSs have been proposed: some of them are presented in Sec. 3, with particular emphasis on the hybrid Method of the Moment (MoM)/Boundary Integral-Resonant Mode Expansion (BI-RME) method, recently developed at the University of Pavia. This method applies to the analysis of thick metal screens perforated periodically with arbitrarily shaped apertures.

Various techniques have been experimented for the fabrication of FSSs: the most suitable technique for a specific application depends on the operation frequency and the required accuracy. The commonly used fabrication techniques both in the GHz and in the THz frequency range are outlined in Sec. 4.1, and discussed at the light of our experience.

The problem of the electrical measurement of samples and prototypes is discussed in Sec. 4.2, with regards to both GHz and THz regions.

Some examples are reported in Sec. 5: the analyses of a dichroic mirror for radioastronomy applications, operating in the X-band, and of a quasi-optical band-pass filter, operating at 280 GHz, are reported and compared with experimental data.

Further author information: (Send correspondence to Maurizio Bozzi)
Maurizio Bozzi: E-mail: m.bozzi@ele.unipv.it, phone: +39 0382505223, fax: +39 0382422583
Luca Perregrini: E-mail: l.perregrini@ele.unipv.it, phone: +39 0382505780, fax: +39 0382422583

Terahertz and Gigahertz Electronics and Photonics II, R. Jennifer Hwu, Ke Wu, Editors,
Proceedings of SPIE Vol. 4111 (2000) © 2000 SPIE. · 0277-786X/00/$15.00

2. OVERVIEW ON FREQUENCY SELECTIVE SURFACES

2.1. Applications of Frequency Selective Surfaces

FSSs have a number of applications in the GHz and in the THz region, for both scientific and commercial purposes.

In the GHz region, FSSs are used as dichroic mirrors in large reflector antennas for radio-astronomy applications.[4–7] The feeding network of such antennas typically consists of beam–waveguide systems (Fig. 1): beams generated by sources operating at different frequencies are combined by FSSs and focused on the main reflector. Another application of FSSs in the GHz region is the band–pass radome[8–10]: at the operating frequency the signal passes through the radome with minimum insertion loss, whereas at out–of–band frequencies the signal is reflected. Moreover, FSSs find a wide commercial use in the screen door of microwave ovens: the perforated metal screen reflects completely the microwave energy at 2.45 GHz, while allowing light to pass through (and, therefore, it allows to see the food inside the oven).

In the THz region, FSSs are used as band–pass filters in quasi–optical systems[11,12] (Fig. 2). In quasi–optical frequency multipliers, FSSs guarantee the required unidirectional operation conditions[13,14]; they may also be used to filter the beam emitted by sources in the millimeter and submillimeter wave range. Other applications of these components in the THz region are in diplexers,[15] in laser cavities,[16] and in Fabry–Perot interferometers.[17]

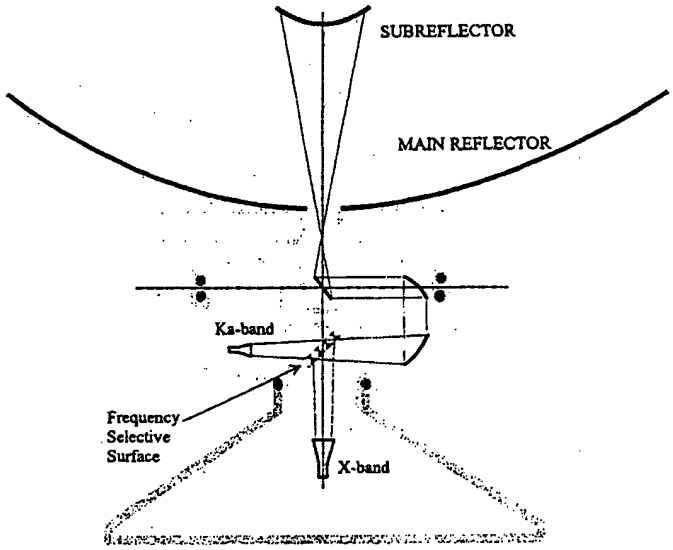

Figure 1. Example of application of FSSs in the beam waveguide of a large reflector antenna: the two beams at X– and Ka–band are combined by an FSS and focused on the main reflector.

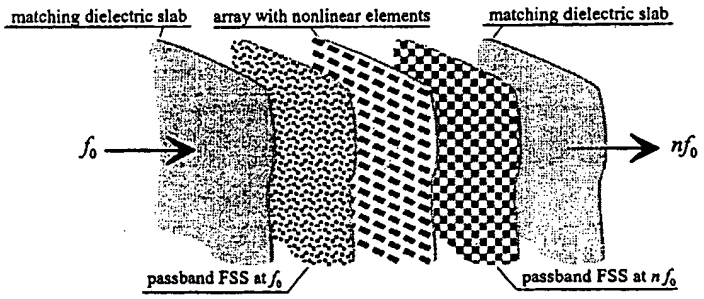

Figur 2. Example of application of FSSs in quasi–optical systems: two bandpass FSSs at f_0 and nf_0 permits to select the input and output frequencies of a quasi–optical frequency multiplier.

2.2. Used Configurations

The most common configuration of FSS consists of a single metal layer, perforated periodically with apertures (Fig. 3). In many cases, the apertures have canonical shapes, such as rectangular[18,19] or circular,[20,21] due to the easier electromagnetic modeling. On the other hand, more complicated shapes are useful for obtaining better performances, such as stability of the resonance frequency with the incident angle, low cross–polarization level, large bandwidth, small band separation. To this aim, crosses,[22,23] Jerusalem crosses,[21,23] tripoles,[22,24] rings and square loops[25,26] have been used.

A multiple screen configuration is sometimes used[27–29]: it consists of two or more perforated metal layers, which are properly stacked (Fig. 4). Multiscreen FSS provides more degrees of freedom, thus enabling to meet the tight design requirements: on the one hand, multiple screen configuration permits to obtain more selective frequency response, on the other hand, it permits to better control both the reflection and the transmission bands.

A double–band frequency response can be achieved by the use of FSSs with multiple apertures per unit cell[30,31] (Fig. 5). FSSs with multiple apertures within a periodic cell present some advantages. In fact, by considering two apertures per unit cell, the FSS can operate in two (closely spaced) frequency bands, and two orthogonal polarizations can be separately adjusted.

Sometimes, metal plates perforated with stepped apertures are used (Fig. 6), especially for radio–astronomy applications[32,33]: they permit to obtain very steep transition from the stop–band to the pass–band, with frequency ratio as small as 1:1.07.[32] This is due to the additional filtering effect of the stepped aperture.

3. ANALYSIS TECHNIQUES

Many numerical methods have been applied in the last decades to the analysis of FSSs. Among them, the most popular are the Finite Difference Time Domain (FDTD) method,[34,35] the Finite Element Method (FEM),[36] the Integral Equation Method (IEM).[37]

The FDTD method and the FEM apply to arbitrary structures, but typically are quite slow. Conversely, the IEM is very efficient if used with entire domain basis functions, whose application, however, is usually limited to particular shapes.[38] On the other hand, sub–domain basis functions (*e.g.* roof–tops) have been typically used in the analysis of arbitrarily shaped apertures, leading to long CPU time and large memory requirement.[21] Recently, we have overcome this drawback by using (also in the case of arbitrarily shaped apertures) entire domain basis functions,[39,11] obtained by the Boundary Integral–Resonant Mode Expansion (BI–RME) method.[40–42] This approach resulted in a fast and flexible computer code, which performs the wideband analysis of FSSs with arbitrarily shaped apertures in tens of seconds on a standard PC. Due to its peculiarity, this code can be effectively embedded in a CAD tool for the analysis and optimization of FSSs.

3.1. MoM/BI–RME Method

The MoM/BI–RME Method permits to calculate the frequency response of FSSs consisting of thin and thick metal screens, perforated periodically with apertures of arbitrary shape, and illuminated by a uniform plane wave.[39,11,31]

Due to the periodicity of the structure, we apply the Floquet theorem and the analysis reduces to the investigation of a single unit cell of the structure. By using the equivalence theorem, the two apertures connecting the waveguide section with the free–space are closed by perfect electric walls, and (unknown) magnetic current densities are defined over the surfaces of the apertures. Thus, the region of interest is split into three parts: the free–space on the two sides of the metal screen and the waveguide section. The fields in free–space are expressed as a combination of Floquet modes, whereas the fields in the waveguide are represented as a combination of the modal fields of the waveguide. The unknown magnetic currents are determined by solving using the MoM the integral equation obtained enforcing the continuity of the tangential components of the fields across the interfaces between the three regions. To represent the unknown magnetic currents we use entire domain basis functions, which are the electric modal fields of the waveguide. The entire domain basis functions are numerically determined in a very efficient way by using the BI–RME method,[40] which is very fast and flexible, and allows for calculating a large number of modes of an arbitrarily shaped waveguide in a few seconds. Furthermore, the method yields as a primary result the boundary values of the potentials of the TE and TM waveguide modes. These results can be used for a direct calculation of the integrals involved in the MoM matrices, by reducing surface to line integrals.[39]

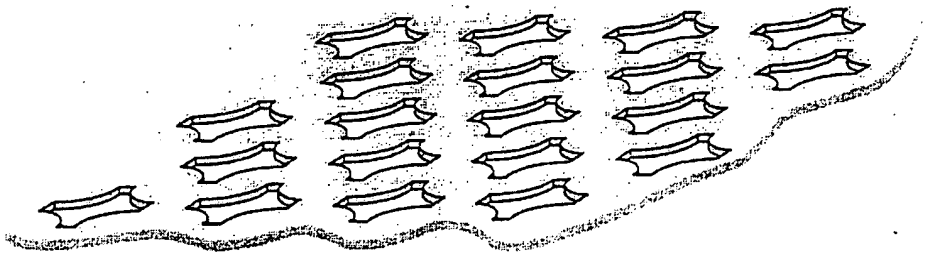

Figure 3. Frequency selective surface consisting of a single layer with arbitrarily shapes apertures.

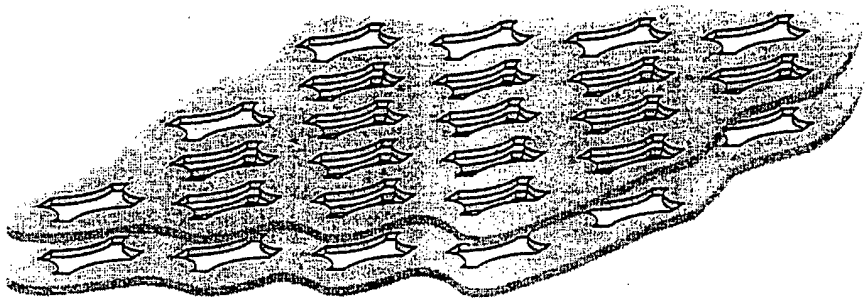

Figure 4. Frequency selective surface consisting of two layers with arbitrarily shapes apertures.

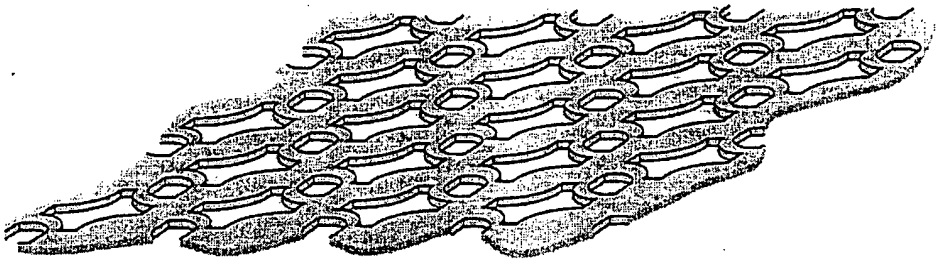

Figure 5. Frequency selective surface consisting of a single layer with more apertures per unit cell.

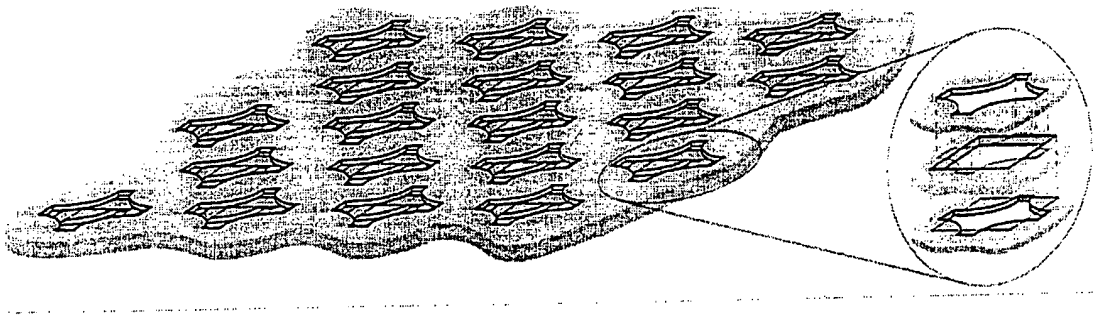

Figure 6. Frequency selective surface consisting of a metal layer with stepped apertures.

The possibility of considering arbitrarily shaped apertures has a tremendous relevance. In fact, it allows for taking into account the unavoidable inaccuracies due to the fabrication process, *e.g.* rounding of edges or corners in the aperture shape (see Sec. 4.1).

4. FABRICATION AND MEASUREMENT OF FREQUENCY SELECTIVE SURFACES

4.1. Fabrication Technologies

The techniques used for the fabrication of FSSs depend on in the dimensions of the structure, and therefore, on the frequency range of application. We experienced many different approaches (such as milling technique, laser cattung, water–jet cutting, chemical etching, and galvanizing growth) for the fabrication of FSSs operating in the GHz and in the Thz region. In the following discussion the advantages and drawbacks of these techniques will be discussed.

In the fabrication of FSS for applications up to 100 GHz the required mechanical accuracy is usually not very high. On the other hand, in these frequency band the structures can be very huge ($3 \times 2m^2$) and thick (up to $3cm$).[6,7] For these reasons, standard mechanical machining techniques are preferred. We used both the milling technique and the water–jet cutting technique, which are able to handle large and thick metallic plates in reasonable time, with good repeatibility and accuracy. The photograph of the prototype of an X–band FSS fabricated by the water–jet cutting technique is shown in Fig. 7. This structure has been designed by CSELT (Turin, Italy) to be used in the beam waveguide of a large reflector antenna for deep space communications (see Fig. 1). These low cost mechanical processes lead to unavoidable fabrication inaccuracies (*e.g.*, the rounding of the corners), which, however, can be accounted for during the analysis based on the MoM/BI–RME method.

When considering higher frequencies ($\geq$ 100 GHz) the typical dimensions of FSS become smaller and photolithographical approaches can be used. As widely discussed in[12] we used both a photolithographical etching process and a galvanizing growth process. The photolithographical etching process proved to be usable for structures operating up to about 200 GHz. Beyond this frequency, the underetching effects lead to a strong deformation of the contour of the apertures. To avoid the underetching problem, we used a galvanizing growth process. With this technique we obtained high accuracy, as shown in Fig. 8 by the photograph of a 280 GHz band–pass filter. With this fabrication technique we realized mesh filters for center frequencies up to 1 THz.

A mechanical approach based on CNC milling machines can be used to fabricate dichroic filters for the THz region.[43] An example of high–pass filter with a cutoff frequency of 1.1 THz fabricated by using this technique is shown in Fig. 9. However, this mechanical technique is limited by its nature to circular apertures with minimum hole diameters due to the finite size of feasible drills. Therefore, limitations are encountered in fabricating dichroic plates with cutoff frequency above $\approx 2THz$. In this frequency range the thickness of the metal plate is below $\approx 70\,\mu m$ allowing the consideration of other fabrication processes like photolithographical, galvanizing growth or, even, laser ablation.

4.2. Measurement Techniques

Even the measurement techniques used for the characterization of FSSs depends on the frequency range. In fact, a widely used technique in the microwave range consists in the measurement of the near field transmitted or scattered by the FSS, and on the calculation of the far field by using standard transformation techniques. This approach permits the measurement of large structures using small anechoic test sites.

On the contrary, a very accurate measurement technique is the THz Time Domain Spectroscopy (THz–TDS). The THz–TDS is based on the excitation of biased semiconductors or electro–optic crystals by a femtosecond laser pulse. In the case of a biased photoconducting material a transient current gives rise to the emission of an electromagnetic (em) pulse of typically less than 1 ps time duration. This em–pulse (THz pulse) comprises a frequency spectrum ranging from a few GHz up to the THz region. Optical sampling permits coherent detection of the electric field strength of the THz pulse, thus enabling the measurement of both the real and imaginary part of the dielectric function of materials. A complete description of the THz–TDS measurement setup is given in.[44–46]

5. ANALYSIS AND EXPERIMENTAL RESULTS

This Section presents the comparison between the simulation results and the experimental data of two FSSs: the former is a dichroic filter for radio–astronomy application operating in the X–band, the latter is a quasi–optical band–pass filter at 280 GHz.

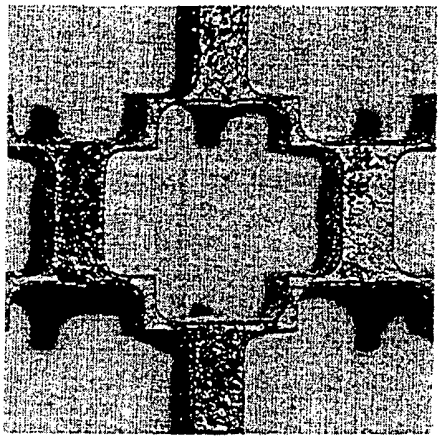

Figure 7. Photograph of a X–band dichroic mirror for radio–astronomy applications, fabricated by water–jet cutting technique [courtesy of CSELT Torino, Italy].

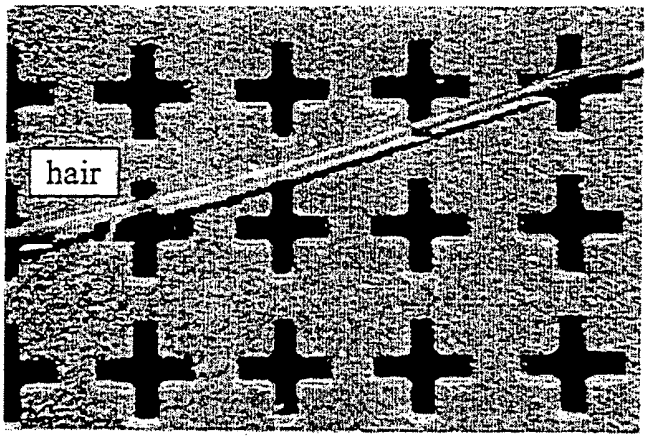

Figure 8. Photograph of a 280 GHz band–pass filter, fabricated by galvanizing growth technique [courtesy of University of Erlangen, Germany].

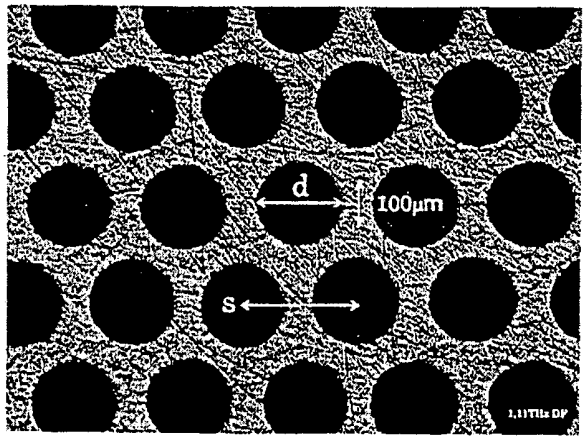

Figure 9. Photograph of a 1.1 THz high–pass filter, fabricated by milling technique [courtesy of University of Freiburg, Germany].

5.1. X–band Dichroic Mirror

The first example refers to the analysis of the dichroic filter presented by Epp *et al.*[5], consisting of a metal plate perforated with cross–shaped apertures (Fig. 10). The analysis of the structure is very challenging, since the plate thickness is comparable with the wavelength and the apertures are tightly packed.

A possible approach to the analysis of dichroic plates perforated with crosses is based on the hypothesis that the thickness w of the metal wall separating the apertures is negligible, and therefore it is set to zero[5]. Under this hypothesis, the currents on the front and back faces of the plate are neglected, and the solution is found by an integral equation method, solved by using the Method of Moments: rooftop basis and razor testing functions are applied. This approach is limited, because the effect of the metal walls is small but not negligible, and plays an important role in the resonant frequencies. Moreover, the analysis is limited to cross–shaped holes defined by a sharp contour. It is not possible, for instance, to take into account the unavoidable rounded corners due to the fabrication process.

By using the MoM analysis powered by the BI–RME method, we performed the analysis of the dichroic filter, considering a finite metal walls ($w = 0.41\ mm$). The simulation results show an excellent agreement with the experimental data[5], for both TE (Fig. 11) and TM polarisation (Fig. 12), considering the incident direction shown in Fig. 10 ($\theta = 30°$, $\phi = 0°$). In the analysis, we used only 35 entire domain basis functions and 400 Floquet modes, and the simulation required 92 *sec* to calculate 50 frequency points on a Sun Ultra 10 workstation.

5.2. 280 *GHz* Band–Pass Filter

The second example refers to the cross shaped band–pass filter[47,12], whose photograph is shown in Fig. 8. By observing the microscope photograph in Fig. 8, we noted the smoothness of the aperture boundary, resulting from the fabrication process. From the photograph, it is possible to deduce that an arc of radius $R = 40\ \mu m$ should be considered instead of the sharp corners.

Therefore, in the MoM/BI–RME analysis, we considered the cross aperture with smoothed corners, drawn in Fig. 13. The dimensions of the cross aperture are reported in the caption of Fig. 13. The thickness of the metal screen is $t = 10\ \mu m$ and the incident field is a vertically polarized uniform plane wave, incident from the normal direction.

We calculated the power transmittance (Fig. 14) and the phase shift (Fig. 15) of the filter in the frequency range 10–1500 *GHz*. The results of the analysis are in excellent agreement with the measurement data in the whole frequency band. In this simulation, we used 26 entire domain basis functions and 425 Floquet modes. The overall computing time on a Sun Ultra 10 workstation was 43 *sec* for the calculation of the frequency response in 150 frequency points.

6. CONCLUSIONS

In this paper we presented an overview of our activity concerning the Frequency Selective Surfaces. In particular, we presented the most important application of FSSs, described the commonly used structures and the numerical methods for their analysis. Among them, we briefly outlined the MoM/BI–RME method, which is a very accurate and flexible hybrid method. Furthermore, we presented the fabrication and measurement techniques suited for the GHz and the THz region. Two examples were reported, showing the accuracy of the code based on the MoM/BI–RME method as well as of the measurement setup.

ACKNOWLEDGMENTS

The authors wish to thank Carsten Winnewisser (University of Freiburg,Germany), Jochen Weinzierl (University of Erlangen, Germany), and Piermario Besso (CSELT Torino, Italy) for providing experimental data and for the fruitful discussions on technological issues.

This work was supported by the European Commission under the TMR Programme "CAD and Verification of mm-wave and Submm-wave Circuits" (contract n. ERBFMRXCT960050) and by the University of Pavia under the Young Researcher Programme and the F.A.R. Funding.

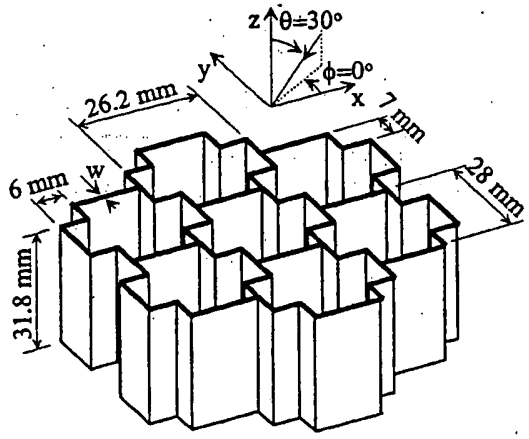

Figure 10. Geometry of the X–band dichroic mirror.

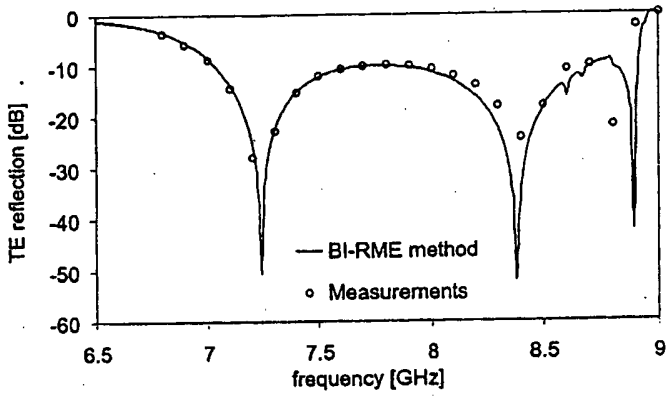

Figure 11. Numerical results for the X–band dichroic mirror, compared with experimental data: amplitude of the reflection coefficient of the TE mode.

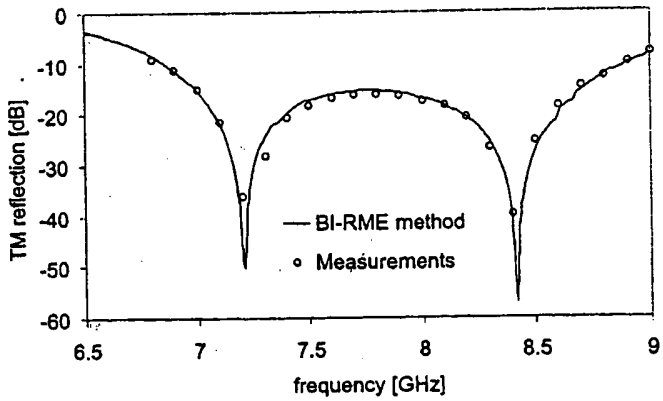

Figure 12. Numerical results for the X–band dichroic mirror, compared with experimental data: amplitude of the reflection coefficient of the TM mode.

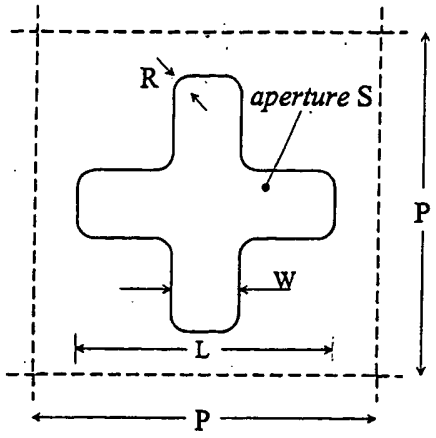

Figure 13. Geometry of the unit cell of the 280 GHz band–pass filter: the aperture shape have rounded corners. Dimensions: $L = 570\ \mu m$, $W = 160\ \mu m$, $R = 40\ \mu m$, $P = 810\ \mu m$; normal incidence is considered.

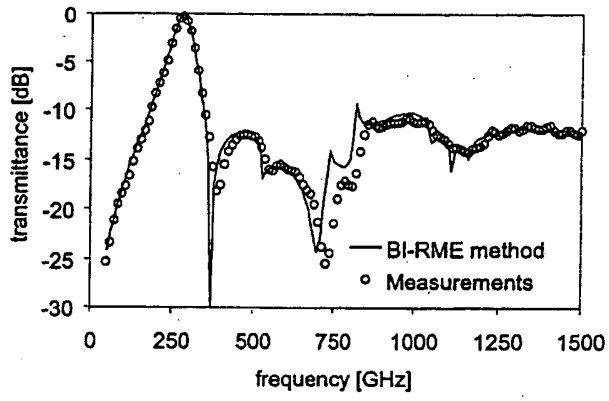

Figure 14. Numerical results for the 280 GHz band–pass filter, compared with experimental data: magnitude of the transmission coefficient.

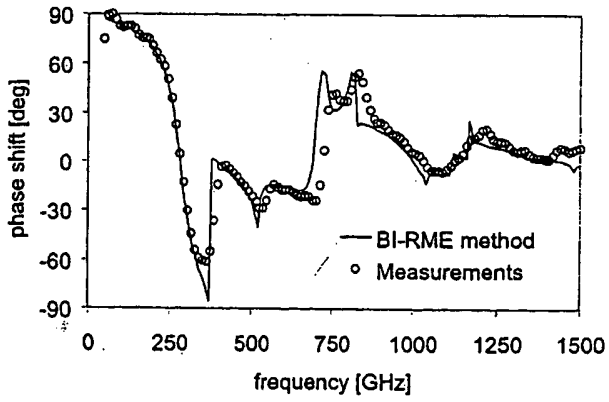

Figure 15. Numerical results for the 280 GHz band–pass filter, compared with experimental data: phase shift of the transmission coefficient.

REFERENCES

1. T. K. Wu, *Frequency Selective Surface and Grid Array*, John Wiley and Sons, 1995.
2. J. C. Vardaxoglou, *Frequency Selective Surfaces*, John Wiley and Sons, 1997.
3. B. Munk, *Frequency Selective Surfaces: Theory and Design*, Wiley Interscience, 2000.
4. R. T. K. Jaldehag, P. S. Kildal, B. O. Ronnang, "Dual-band Reflector Feed System for Classical Cassegrain Radio Telescopes," *IEEE Trans. Antennas & Propagat.*, **41**, pp. 325–332, 1993.
5. L. W. Epp, P. H. Stanton, R. E. Jorgenson, and R. Mittra, "Experimental Verification of an Integral Equation Solution for a Thin-Walled Dichroic Plate with Cross-Shaped Holes," *IEEE Trans. Antennas & Propagat.*, **42**, pp. 878–882, 1994.
6. P. Besso, M. Bozzi, P. Gianola, R. Maddè, L. Perregrini, and L. Salghetti Drioli, "Design of Dichroic Filters for Deep Space Antennas," *Proc. of 2000 AP-S/URSI Symp*, Salt Lake City, USA, 2000.
7. P. Besso, M. Bozzi, M. Brenner, S. Junker, R. Maddè, L. Perregrini, and L. Salghetti Drioli, "Electrical and Mechanical Performance of a S/X/Ka–Band Dichroic Mirror," *Proc. of 2000 European Microwave Conference*, Paris, France, 2000.
8. E. L. Pelton, B. A. Munk, "A streamlined metallic radome," *IEEE Trans. Antennas & Propagat.*, **22**, pp. 799-8.3, 1974.
9. A. Roberts, R. C. McPhedran, "Bandpass grids with annular apertures," *IEEE Trans. Antennas & Propagat.*, **36**, pp. 607–611, 1988.
10. T. K. Wu, "High Q bandpass structure for the selective transmission and reflection of high frequency radio signals," *US Patent 5,103,241*, 1992.
11. M. Bozzi, L. Perregrini, J. Weinzierl, and C. Winnewisser, "Analysis of Frequency Selective Surfaces for Quasi–Optical Applications," in *Terahertz and Gigahertz Photonics, Proc. SPIE* **3795**, pp. 322-328, 1999.
12. M. Bozzi, L. Perregrini, J. Weinzierl, and C. Winnewisser, "Design, Fabrication and Measurement of Frequency Selective Surfaces," *Optical Engineering*, **39**, 2000.
13. P. Arcioni, M. Bozzi, G. Conciauro, and L. Perregrini, "Design and Optimization of Quasi–Optical Frequency Multipliers," *Intern. Journal of Infrared and Millimeter Waves*, **20**, pp. 913-928, 1999.
14. F. Maiwald, F. Lewen, B. Vowinkel, W. Jabs, D.G. Paveljev, M. Winnewisser, and G. Winnewisser, "Planar Schottky Diode Frequency–Multiplier for Molecular Spectroscopy up to 1.3 THz," *IEEE Microwave and Guided Wave Lett.*, **9**, pp. 198–200, 1999.
15. C. Letrou and M. Gheudin, "Dichroic Diplexer Design for Millimeter Waves," *Intern. Journal of Infrared and Millimeter Waves* **13**, pp. 27–42, 1992.
16. D. A. Weitz, W. J. Skocpol, and M. Tinkham, "Capacitive–mesh output couplers for optically pumped far–infrared lasers," *Opt. Lett.* **3**, pp. 13–15, 1978.
17. R. D. Rawcliffe and C. M. Randall, "Metal mesh interference filters for the far infrared," *Appl. Opt.* **6**, pp. 1353–1358, 1967.
18. C. C. Chen, "Transmission Through a Conductive Screen Perforated Periodically with Apertures," *IEEE Trans. Microwave Theory & Tech.*, **18**, pp. 627–632, 1970.
19. S. W. Schneider and B. A. Munk, "The scattering properties of "Super Dense" arrays of dipoles," *IEEE Trans. Antennas & Propagat.*, **42**, pp. 463–472, 1994.
20. C. C. Chen, "Diffraction of Electromagnetic Waves by a Conducting Screen Perforated Periodically with Circular Holes," *IEEE Trans. Microwave Theory & Tech.*, **19**, pp. 475–481, 1971.
21. R. Mittra, C. H. Chan, and T. Cwik, "Techniques for Analyzing Frequency Selective Surfaces–A Review," *Proc. of the IEEE* **76**, pp. 1593–1615, 1988.
22. E. L. Pelton and B. A. Munk, "Scattering from Periodic Arrays of Cross Dipoles," *IEEE Trans. Antennas & Propagat.*, **27**, pp. 323–330, 1979.
23. C. H. Tsao and R. Mittra, "Spectral–Domain Analysis of Frequency Selective Surfaces Comprised of Periodic Arrays of Cross Dipoles and Jerusalem Crosses," *IEEE Trans. Antennas & Propagat.*, **32**, pp. 478–486, 1984.
24. J. C. Vardaxoglou and E. A. Parker, "Performance of two tripole arrays as frequency selective surfaces," *Electron. Lett.*, **19**, pp. 709–710, 1983.
25. J. Huang, T. K. Wu, and S. W. Lee, "Tri–band Frequency Selective Surface with Circular Ring Elements," *IEEE Trans. Antennas & Propagat.*, **42**, pp. 166–175, 1994.

26. T. K. Wu, "Single-Screen Triband Frequency Selective Surface with Double-Square-Loop Elements," *Microwave and Optical Technology Letters*, **5**, pp. 56–59, 1992.
27. S. Contu and R. Tascone, "Scattering from Passive Arrays in Plane Stratified Regions," *Electromagnetics*, 5, pp. 285–306, 1985.
28. C. Antonopoulos, R. Cahill, E. A. Parker, and I. M. Sturland, "Multilayer Frequency–Selective Surfaces for Millimetre and Submillimetre Wave Applications," *IEE Proc.-Microw. Antenna Propag.*, **144**, pp. 415–420, 1997.
29. R. Sauleau, Ph. Coquet, J. P. Daniel, T. Matsui, and N. Hirose, "Analysis of Millimeter–Wave Fabry–Perot Cavities Using the FDTD Technique," *IEEE Microwave and Guided Wave Letters*, **9**, pp. 189–191, 1999.
30. J. A. Reed and D. M. Byrne, "Frequency–Selective Surfaces with Multiple Apertures Within a Periodic Cell," *J. Opt. Soc. Am. A*, **15**, pp. 660–668, 1998.
31. M. Bozzi and L. Perregrini, "Analysis of FSS with Multiple, Arbitrarily Shaped Elements Within a Periodic Cell," *Proc. of 2000 AP-S/URSI Symp*, Salt Lake City, USA, 2000.
32. J. C. Chen, P. H. Stanton, and H. F. Reilly, Jr., "A Prototype Ka–/Ka–Band Dichroic Plate With Stepped Rectangular Apertures," *Jet Propulsion Laboratory, TDA Progress Report*, **42–124**, pp. 143–152, 1996.
33. W. A. Imbriale, "A New All–Metal Low–Pass Dichroic Plate," *Jet Propulsion Laboratory, TDA Progress Report*, **42–129**, pp. 1–10, 1997.
34. P. Harms, R. Mittra, Ko Wai, "Implementation of the periodic boundary condition in the finite–difference time–domain algorithm for FSS structures," *IEEE Trans. Antennas Propagat.* **42**, pp.1317–1324, 1994.
35. W. Yu, S. Dey, R. Mittra, "Modeling of periodic structures using the finite difference time domain (FDTD)," *Proc. of 1999 AP-S/URSI Symp*, pp. 594–597, 1999.
36. M. Lambea, M. A. Gonzalez, J. A. Encinar, J. Zapata, "Analysis of frequency selective surfaces with arbitrarily shaped apertures by finite element method and generalized scattering matrix," *IEEE APS International Symposium 1995 Digest* 3, pp. 1644–1647, 1995.
37. T. F. Eibert, J. L. Volakis, D. R. Wilton, D. R. Jackson, "Hybrid FE/BI modeling of 3–D doubly periodic structures utilizing triangular prismatic elements and an MPIE formulation accelerated by the Ewald transformation," *IEEE Trans. Antennas Propagat.* **47**, pp. 843–850, 1999.
38. C. C. Chen, "Transmission of Microwave Through Perforated Flat Plates of Finite Thickness," *IEEE Trans. Microwave Theory Tech.* **21**, pp. 1–6, 1973.
39. M. Bozzi and L. Perregrini, "Efficient Analysis of Thin Conductive Screens Perforated Periodically with Arbitrarily Shaped Apertures," *Electron. Lett.*, **35**, No. 13, June 1999.
40. G. Conciauro, M. Guglielmi, and R. Sorrentino, *Advanced Modal Analysis*, John Wiley and Sons, 1999.
41. G. Conciauro, P. Arcioni, M. Bressan, and L. Perregrini, "Wideband Modeling of Arbitrarily Shaped H-Plane Waveguide Components by the 'Boundary Integral-Resonant Mode Expansion Method'," *IEEE Trans. Microwave Theory Tech.*, **44**, pp. 1057-1066, July 1996.
42. P. Arcioni, M. Bressan, G. Conciauro, and L. Perregrini, "Wideband Modeling of Arbitrarily Shaped E-Plane Waveguide Components by the 'Boundary Integral-Resonant Mode Expansion Method'," *IEEE Trans. Microwave Theory Tech.*, **44**, pp. 2083-2092, Nov. 1996.
43. C. Winnewisser, F. Lewen, J. Weinzierl, and H. Helm, "Transmission features of frequency–selective components in the far infrared determined by terahertz time–domain spectroscopy," *Appl. Optics* **38**, pp. 3961–3967, 1999.
44. A. Gürtler, C. Winnewisser, H. Helm, and P. Uhd Jepsen, "Terahertz pulse propagation in the near and far field," *J. Opt. Soc. Am. A* **17**, 2000.
45. C. Winnewisser, F. Lewen, and H. Helm, "Transmission characteristics of dichroic filters measured by THz time–domain spectroscopy," *Appl. Phys. A* **66**, pp. 593–598, 1998.
46. C. Winnewisser, F. Lewen, M. Schall, M. Walther, and H. Helm, "Characterisation and Application of Dichroic Filters in the 0.1 to 2 THz Region," *IEEE Trans. on Microwave Theory Tech.* **48**, 2000.
47. D. Steup and J. Weinzierl, "Resonant THz–Meshes," *Proc. of the 4th Intern. THz Workshop*, Erlangen–Tennenlohe, Germany, 1996.